ACS OMEGA

http://pubs.acs.org/journal/acsodf

Article

Association Reaction of Gaseous C_2H_4 in Femtosecond Laser Filaments Studied by Time-of-Flight Mass Spectrometry

Akitaka Matsuda,* Kentaro Tani, Yukari Takeuchi, Yui Hayakawa, and Akiyoshi Hishikawa*

Cite This: *ACS Omega* 2021, 6, 29862−29868

Read Online

ACCESS | Metrics & More | Article Recommendations | Supporting Information

ABSTRACT: Association reactions by femtosecond laser filamentation in gaseous C_2H_4 were studied by time-of-flight mass spectrometry of neutral reaction products. Direct sampling from the reaction cell to a mass spectrometer via a differential pumping stage allowed the identification of various hydrocarbon molecules C_nH_m with n = 3−7 and m = 4−7, which includes species not observed in the previous studies. It was found that products containing three and four carbon atoms dominate the mass spectrum with smaller yields for higher-mass species, suggesting that carbon chain growth proceeds through the reaction with C_2H_4 in the reaction cell. The product distribution showed a clear dependence on the laser pulse energy for filamentation.

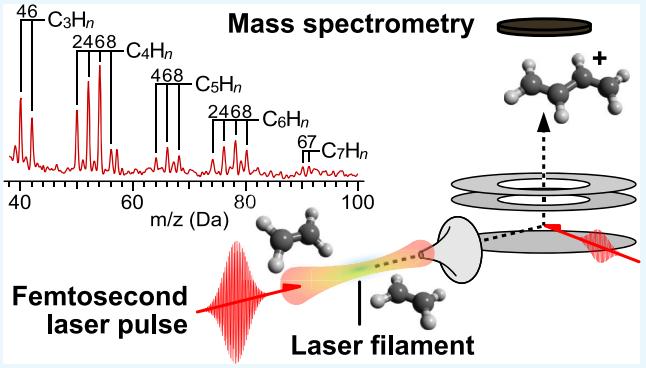

1. INTRODUCTION

Ultrashort intense laser fields provide unique methods in controlling the reaction dynamics via strong interaction with the valence electrons of molecules.[1,2] Combined with coherent pulse-shaping techniques, the intense-field control has been demonstrated successfully for unimolecular reactions accompanying bond scission and rearrangement.[3−8] During the last decade, intense laser pulses have also been utilized to manipulate many-body reactions, in particular by using femtosecond laser filaments. The laser filament is formed by loose focusing of ultrashort laser pulses in a medium. The laser field intensity in a filament is clamped to ∼10^{14} W/cm^2 and maintained over a long distance because of the competition between self-focusing by the Kerr lens and defocusing induced by the plasma formation.[9−11] Many-body reactions by laser filamentation have been demonstrated in gas[12−19] and liquid phases.[20−25] For example, the formation of nanoparticles, such as amorphous carbon nanospheres from CH_4[15] and amorphous aluminum-carbide and aluminum-magnesium-carbide nanoparticles from $Al(CH_3)_3$ and $Al_2Mg(CH_3)_8$[16] were reported. Synthesis of small molecules, CO_2 and C_2H_2, was demonstrated by laser filamentation in a gas mixture of CO and H_2.[13]

Laser filament reactions in gaseous C_2H_4 have been subjected to several studies.[18,19] The chemical structures and morphology of the precipitates were investigated by Raman/fluorescence spectroscopy, X-ray photoelectron spectroscopy, transmission electron microscopy, electron diffraction, and electron energy loss spectroscopy.[18] It was found that the precipitates consist of hydrogenated amorphous carbon films and nanoparticles and that the laser field intensity is an important parameter to control their sp^2/sp^3 structure and particle size distribution.[18] More recently, a gas flow experiment[19] was carried out to collect the reaction products from laser filaments in a cooled solvent, where the formation of hydrogen-capped polyynes, $C_{2n}H_2$ (n = 3−6), was observed by UV absorption spectroscopy.

Compared with these experiments studying products recovered in the form of solids or solutions, direct sampling of reaction intermediates and nascent products should be useful to gain further understanding of the many-body reactions induced by laser filaments. UV/vis absorption spectroscopy is a powerful tool for this purpose, as demonstrated in the analysis of gaseous products by laser filamentation in air.[26,27] The products were sampled to separate UV analyzers for ozone and nitrogen oxides to determine their local concentration to understand the underlying mechanism of water condensation.[26] In situ measurements such as cavity ring-down spectroscopy[27] and emission spectroscopy[28] have also been utilized to directly evaluate the total yield of the products in the sample cell.

Though useful in the quantitative analysis of products, the absorption and emission spectroscopies are often limited in the range of applicability because light sources, optics, and detectors need to be properly prepared for the species of

Received: August 12, 2021
Accepted: September 30, 2021
Published: October 29, 2021

https://doi.org/10.1021/acsomega.1c04354
ACS Omega 2021, 6, 29862−29868

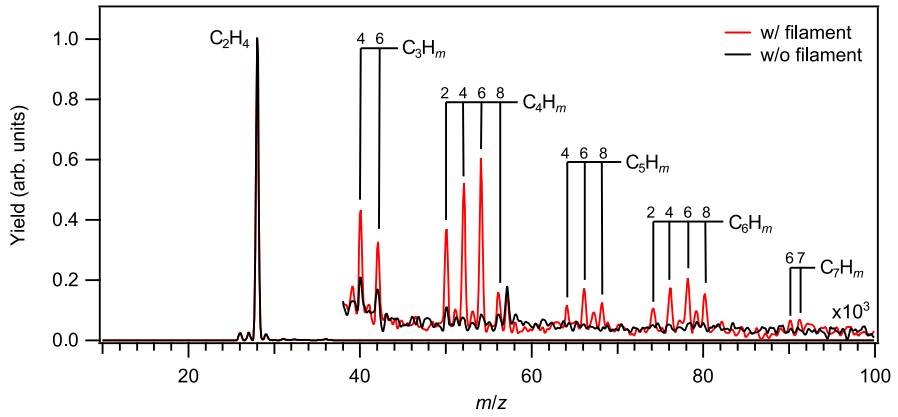

Figure 1. Mass spectra normalized at m/z 28, obtained with (red) and without (black) the filament laser pulse (340 μJ/pulse). The assignments of the peaks observed with the filament pulse are shown. Note that the peaks at m/z 40, 42, and 57 in the spectra, observed without the laser filament pulse (black), originate from the residual gas inside the time-of-flight mass spectrometer and that at m/z 50 is attributed to a contaminant in the sample gas.

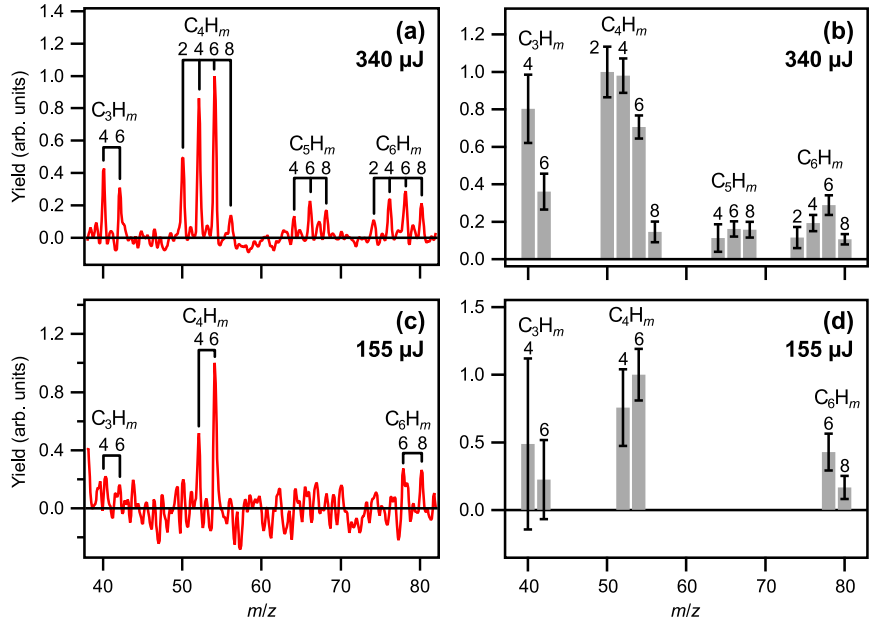

Figure 2. Differential spectrum obtained for filament laser energies of (a) 340 and (c) 155 μJ/pulse. Relative yield of the molecular products with even m/z after tunneling ionization probability correction for filament laser energies of (b) 340 and (d) 155 μJ/pulse.

interest. Mass spectrometry offers an alternative tool capable of the simultaneous detection of a wide range of products. It has been applied to identify products from the synthesis gas,[13] where a cell filled with the gaseous reactants was irradiated with intense laser pulses for hours, and the gaseous products were sampled by a syringe to a mass spectrometer.[13] A similar sample analysis was carried out for laser filaments in CH_4, where C_2H_2, C_2H_4, C_3H_4, C_4H_2, C_5H_6, C_6H_2, and C_6H_6 were observed.[15] A more direct sampling of the products has been conducted for a laser filament in air, where a filament was formed in the ion-extraction region of a time-of-flight spectrometer to identify ionic products such as O_3^+ and HNO_3^+.[29] Here, we have developed another mass spectrometric approach to sample neutral products from a laser filament in gas through a differential pumping stage separating a reaction cell and a mass spectrometer. We apply this method to identify neutral products from C_2H_4 to understand the reaction process in the laser filaments.[18,19] We found that various hydrocarbon species were formed, including hydrogen-capped polyynes. Linear carbon chains[30] and small carbon clusters[31] are of great interest not only in materials science due to the unique property of carbon nanomaterials but also in molecular astrophysics as carbonaceous hydrocarbon molecules are found in the interstellar medium.[32]

2. RESULTS AND DISCUSSION

Typical mass spectra obtained in the experiment are shown in Figure 1. The spectrum obtained with the probe pulse alone (black line) is dominated by a peak at m/z 28, corresponding to $C_2H_4^+$, produced by the ionization of the reactant ethylene. The peaks observed at m/z 27 and 26 are assigned to $C_2H_3^+$ and $C_2H_2^+$ fragment ions produced by the dissociative ionization of ethylene by the probe pulse. The peak at m/z 29 is assigned to an isotopomer of ethylene. Figure 1 also displays the mass spectrum obtained with both the filament and probe pulse normalized by the $C_2H_4^+$ peak (red line). These two spectra look almost the same, but a careful inspection of the higher-mass region (m/z 40−100) reveals

https://doi.org/10.1021/acsomega.1c04354
ACS Omega 2021, 6, 29862−29868

Table 1. Ionization Energies I_p,[33−37] Tunnel Ionization Rate Γ, and Ionization Probability P of Selected Molecules

m/z	formula	compound	I_p (eV)	Γ[a] (×10^{14} s^{-1})	P[b]
28	C_2H_4	ethylene	10.5	0.781	0.089
40	C_3H_4	propyne	10.4	0.930	0.11
42	C_3H_6	propene	9.7	3.13	0.40
50	C_4H_2	1,3-butadiyne	10.2	1.32	0.16
52	C_4H_4	1-buten-3-yne	9.6	3.72	0.46
54	C_4H_6	1,3-butadiene	9.0	10.4	0.89
56	C_4H_8	2-butene	9.1	8.76	0.83
		1-butene	9.6	3.72	0.46
64	C_5H_4	1,3-pentadiyne	9.5	4.41	0.54
		1,4-pentadiyne	10.3	1.11	0.13
66	C_5H_6	1,3-cyclopentadiene	8.6	20.5	0.99
		1-penten-3-yne	9.1	8.76	0.83
		3-penten-1-yne	9.2	7.38	0.76
		1-buten-3-yne, 2-methyl-	9.3	6.22	0.69
68	C_5H_8	1,3-pentadiene	8.7	17.3	0.98
		isoprene	8.9	12.3	0.93
		cyclopentene	9.0	10.4	0.89
		2-pentyne	9.4	5.24	0.61
		1,4-pentadiene	9.6	3.72	0.46
		1-butyne, 3-methyl-	10.0	1.86	0.24
		1-pentyne	10.1	1.57	0.20
74	C_6H_2	1,3,5-hexatriyne	9.5	4.41	0.54
76	C_6H_4	benzyne	9.0	10.4	0.89
		hexa-1,5-diyne-3-ene	9.1	8.76	0.83
78	C_6H_6	1,5-hexadien-e-yne	8.5	24.3	1.0
		2,4-hexadiyne	8.9	12.3	0.93
		1,3-hexadien-5-yne	9.2	7.38	0.76
		benzene	9.3	6.22	0.69
		1,3-hexadiyne	9.4	5.24	0.61
		1,4-hexadiyne	9.7	3.13	0.40
		1,5-hexadiyne	9.9	2.22	0.28
80	C_6H_8	1,3-cyclohexadiene	8.3	34.1	1.0
		1,3,5-hexatriene	8.3	34.1	1.0
		1,3-cyclopentadiene, 1-methyl-	8.4	28.8	1.0
		2-methyl-1,3-cyclopentadiene	8.4	28.8	1.0
		1,3-cyclopentadiene, 5-methyl-	8.5	24.3	1.0
		1,4-cyclohexadiene	8.8	14.6	0.96
		1-hexen-3-yne	8.9	12.3	0.93

[a]Calculated at F = 0.048 au (I = 8.2 × 10^{13} W/cm^2). [b]Calculated for the probe pulse with the duration of 50 fs and the peak intensity of 8.2 × 10^{13} W/cm^2.

that many new peaks appear when the filament laser is turned on. The new peaks are assigned to hydrocarbon molecules larger than C_2H_4 formed in the filament. The difference spectrum is shown in Figure 2a. The mass spectrum is dominated by products with even mass numbers, indicating that the hydrocarbons containing an even number of hydrogen atoms are the major reaction intermediates and products. Strong peaks observed at m/z 50−54 in the difference spectrum are assigned to C_4H_m (m = 2, 4, and 6). The weaker peaks at m/z ∼40 are hydrocarbon molecules containing three carbon atoms, C_3H_m (m = 4 and 6). The peaks at m/z ∼66 and ∼78 are C_5H_m (m = 4, 6, and 8) and C_6H_m (m = 2, 4, 6, and 8), respectively. In addition to these peaks, weak signals observed around m/z 90 may be attributed to C_7H_m (m = 6 and 7). No clear peaks are seen in the mass range higher than m/z 94.

In the present study, intense laser pulses are used to ionize the reaction products for mass spectroscopy. The field intensity at the focal spot is estimated to be 8.2 × 10^{13} W/cm^2, showing that the tunneling ionization is predominant in the ionization process. Since the tunneling ionization rate depends on the ionization potential I_p, the ionization efficiency of each species should be taken into account for a more quantitative discussion. Table 1 lists the tunneling ionization rates Γ calculated using the following equation[38,39]

$$\Gamma = \frac{B(m)^2}{2^{|m|}|m|!}\frac{1}{\kappa^{2/\kappa-1}}\left(\frac{2\kappa^3}{F}\right)^{2/\kappa-|m|-1}\exp\left(-\frac{2\kappa^3}{3F}\right) \quad (1)$$

for species relevant to the present study, where $\kappa = \sqrt{2I_p}$ and F is the field intensity. F = 0.048 au at the peak laser field intensity of 8.2 × 10^{13} W/cm^2. The $B(m)$ coefficients are calculated according to ref 39, with l = 1 and $|m|$ = 1. Structure factors unique to each species are not considered for simplicity. The ionization energies are adopted from refs 33−37. The results show a general trend that species with larger masses have smaller ionization potentials, which results in larger ionization rates. The ionization probability P can be obtained

https://doi.org/10.1021/acsomega.1c04354
ACS Omega 2021, 6, 29862−29868

by the time integration of the tunneling rate over the probe pulse[40]

$$P = 1 - \exp\left[-\int_{-\infty}^{\infty} \Gamma(F(t))\mathrm{d}t\right] \quad (2)$$

where $F(t)$ is the instantaneous laser electric field at time t of the probe pulse, where a Gaussian intensity profile is assumed. The obtained values are tabulated in Table 1. Furthermore, the variation of the field intensity near the focal spot is also taken into account. By integration over the volume V, the ionization yield S is expressed as[41]

$$S = D\int_0^{I_0} P(I)\left(-\frac{\partial V}{\partial I}\right)\mathrm{d}I \quad (3)$$

where D denotes the density of the target molecules in the interaction region and $\left(-\frac{\partial V}{\partial I}\right)\mathrm{d}I$ represents the volume element. Figure 2b shows the relative yields of the products corrected for the ionization efficiencies. For a mass assignable to different species, the average of the corresponding ionization efficiencies is used for simplicity. After the correction, the product yields of C_3H_{2m} is comparable to those of C_4H_{2m}, while the yields of C_5H_{2m} and C_6H_{2m} are distinctively smaller. A similar spectrum was obtained at a lower probe pulse energy of 7.4 μJ (Figure S1). Although fragmentation associated with the ionization process by the probe pulse should be taken into account for quantitative discussions as in the case of other mass spectrometric studies,[42] the observed results suggest that the chain growth reaction proceeds mainly through a sequential reaction with species containing two carbon atoms, for example, neutral ethylene abundant in the reaction cell, to reaction intermediates.

In the previous UV spectroscopic study of the recovered products from a laser filament in ethylene, the production of polyynes $C_{2n}H_2$ (n = 3−6) was identified.[19] In the present study, the lowest member of the polyyne, C_6H_2, is clearly observed at m/z 74 together with other products containing six carbon atoms C_6H_m (m = 4, 6, and 8). On the other hand, products with masses higher than m/z 93 including polyynes, C_nH_2 (n = 8, 10, and 12), were not observed. The difference from the previous study[19] could be interpreted as a result of the direct sampling of nascent products, which suppress possible secondary reactions in the cold solvent trap. Another major difference between the two studies is the laser field intensity of the pump pulse, which is estimated to be smaller by an order of magnitude in the current experiment. In order to clarify the effect of the laser field intensity dependence, mass spectrum is recorded at a lower intensity (155 μJ/pulse), as shown in Figure 3. The field intensity was chosen to avoid any precipitation[18] onto the small orifice which will seriously affect the gas flow. In the obtained spectra, the C_4H_4 and C_4H_6 products remain observed. However, the peaks with m/z higher than 60 decreased significantly and buried in the background noise, thus showing a clear effect of the laser field intensity on the generated molecules. Interestingly, the distribution in the C_4H_m products differs from that obtained at the higher pulse energy (Figure 2a), which might be interpreted in terms of the complex dynamics of micro-plasma.[43]

In a laser filament, strong interaction between the target molecule and the laser field produces intermediates, such as molecular and fragment ions[44] and neutral fragments.[45] They react with other species in the cell to form product molecules.

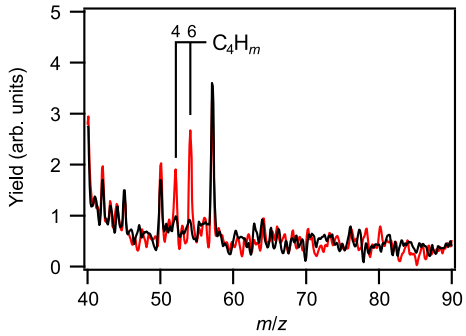

Figure 3. Mass spectra obtained with (red) and without (black) the filament laser pulse (155 μJ/pulse).

Since multiple collisions are necessary to produce molecules with larger masses ($m/z \gtrsim 60$) from ethylene, the product yields should decrease with the increase in the mass. This explains the overall trend observed in the mass spectrum in Figure 1. In addition, since the generation of reaction intermediates is a highly nonlinear process,[44,45] the yield of higher-mass products is expected to decrease drastically by a decrease in the laser field intensity, which explains the significant suppression of heavier products at the low field intensity (Figure 3).

The relative yield of the products generated by laser filamentation at lower field intensity is shown in Figure 2d. While sharp peaks are observed for C_4H_4 and C_4H_6 in the differential spectrum (Figure 2c), it appears that other products are barely formed. This suggests that the decrease in the laser intensity not only leads to the suppression of C_5H_m and C_6H_m but also affects the generation of C_3H_m. It is possible that C_3H_m is formed by the dissociation of C_4H_m or larger species by succeeding filamentation laser pulses at higher field intensity.[46] Alternatively, the increased yields of C_3H_m could be interpreted in terms of the changes in the distribution of reaction intermediates formed in the filament. It is established that intermediates containing one carbon atom (CH_m) is formed more efficiently at a higher field intensity.[44] If the formation of C_3H_m proceeds by a binary collision between CH_m and ethylene, the yield of C_3H_m should increase as the field intensity increases.

Photolysis of ethylene has been studied in the vacuum ultraviolet (VUV) region.[47] Gas chromatography of the products obtained by the many-body reaction by VUV light irradiation revealed that four-carbon molecules containing a larger number of hydrogen atoms, C_4H_m (m = 6, 8, and 10), are the dominant products, suggesting that the association reaction product yield is different from that in the present case. This difference in the distribution of the obtained products can be interpreted by the difference in the initial fragmentation process. In the VUV photolysis, C_2H_3 and C_2H_2 are the major fragments. It is proposed that the most major product C_4H_8 is formed by $C_2H_3 + C_2H_5 \rightarrow C_4H_8$, where the ethyl radical C_2H_5 is produced by the reaction between C_2H_4 and the H fragment, $C_2H_4 + H \xrightarrow{+M} C_2H_5$. In the present case, a variety of species with fewer hydrogen atoms, such as C_2, CH, C_2H^+, C_2^+, CH^+, and C^+, are produced in intense laser fields.[44,45] A reaction such as $C_2H_4 + C_2 \rightarrow C_4H_4$ may take place to form C_4H_4 in the femtosecond laser filament. This suggests that such fragments are required to form the major products, C_3H_4, C_4H_2, and C_4H_4, as well as C_5H_m and C_6H_m in laser filaments,

https://doi.org/10.1021/acsomega.1c04354
ACS Omega 2021, 6, 29862−29868

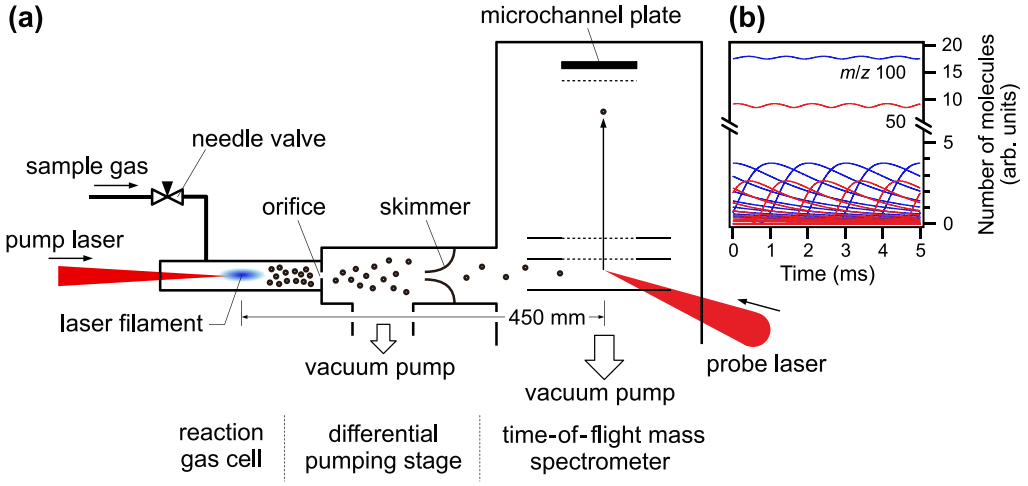

Figure 4. (a) Schematic of the experimental apparatus. The setup consists of three stages, a reaction gas cell, a differential pumping stage, and a Wiley−McLaren-type time-of-flight mass spectrometer (see the text for details). (b) Time profile of the number of molecules reaching the mass spectrometer, simulated for m/z 50 and 100. Maxwell−Boltzmann velocity distribution at 298 K was assumed. Superposition of products formed by successive laser pulses (bottom) creates a quasi-continuous beam to the mass spectrometer (top).

indicating the uniqueness of the chemical reactions in laser filaments.

3. SUMMARY

We have developed a time-of-flight mass spectrometric technique to investigate reaction intermediates and products from femtosecond laser filaments formed by loose focussing of intense laser pulses to a gaseous medium. Products from a filament were sampled to a mass spectrometer via a differential pumping stage connected to a reaction cell. Mass spectrometry has been applied to the filament-induced reactions in C_2H_4. Identification of hydrocarbon species from C_3H_4 to C_7H_7, which were not observed in the previous study on recovered samples, was demonstrated. The observed mass spectra were dominated by signals from C_4H_m (m = 2, 4, and 6). A clear dependence on the laser pulse energy for the filamentation was observed, showing a growth of higher-mass products with an increase in the pulse energy. The increase was also observed for a small-mass species C_3H_m (m = 4 and 6), suggesting a reaction process involving small reaction intermediates produced by the significant fragmentation of C_2H_4 in intense laser fields. Mass spectrometry of reaction products from laser filaments will provide a deeper understanding of the reaction mechanism of other gaseous media investigated in the previous studies[13,15−17,25−27] and suggest a way to control the many-body reactions by laser pulse manipulation.

4. EXPERIMENTAL METHOD

The schematic of the experimental setup is shown in Figure 4a. The setup consists of a reaction gas cell, a differential pumping stage, and a Wiley−McLaren-type time-of-flight mass spectrometer. The output from a femtosecond Ti:sapphire laser amplifier system (800 nm, 50 fs, 1 kHz) was divided into two by a beam splitter (34:1). The main pulse was focused by a plano-convex lens (f = 200 mm) into the reaction cell to generate a laser filament. The other (10 μJ/pulse) was focused into the mass spectrometer with a plano-convex lens (f = 200 mm) for the ionization of products. The gaseous products from the laser filament is sampled to the mass spectrometer through an orifice (200 μm) and a skimmer (200 μm) placed at the entrance and the exit of the differential pumping stage, respectively. The C_2H_4 gas (99.9% purity, Takachiho Chemical Industrial) was continuously supplied to the reaction cell without any further purification. The pressures inside the gas cell, differential pumping chamber, and mass spectrometer were maintained at 6×10^4 Pa, 2×10^1 Pa, and 9×10^{-4} Pa, respectively, where a 500 L/min dry scroll pump was used for differential pumping and two turbo molecular pumps (480 and 67 L/s) were used for the mass spectrometer. The flow rate of the sample gas is estimated from the pressure difference to be 250 mL/min. The distance between the reaction region and the probe ionization region was approximately 450 mm, which results in a time delay of 1.5 ns between the filamentation and probe pulse at their respective interaction regions. While the transit time for a product molecule to travel from the reaction chamber to the mass spectrometer varies with the mass, it is approximately 1−2 ms for m/z 28−100 at room temperature. This indicates that the products from the filaments are ionized by the pulses proceeding to the filamentation pulse in the pulse train generated at the 1 kHz repetition rate. Since the velocity distributions at room temperature are broad enough, each product species propagates as a quasi-continuous beam to the mass spectrometer (see Figure 4b). The ionized molecule is guided to the microchannel plate detector (C0701, Jordan TOF Products) by the static field generated by the electrodes. After the amplification (SR455A, Stanford Research Systems) and discrimination (model 935, Ortec), the signal from the detector was recorded by a time-to-digital converter (TDC8, RoentDek). The mass spectra with and without the filament laser pulse in the cell were acquired every other ∼30 min. The reaction gas cell was evacuated and cleaned after each measurement cycle. The energy of the pump laser pulse was varied by using a neutral density filter. Although the filament field intensity is difficult to be determined in the present case, the previous study in air[48] suggests that the pulse energies (340 and 155 μJ/pulse) and the focal length (f = 200 mm) are well below the clamping conditions. Indeed, the mass spectra recorded at these conditions show different distributions (Figures 1 and 3).

https://doi.org/10.1021/acsomega.1c04354
ACS Omega 2021, 6, 29862−29868

■ ASSOCIATED CONTENT

Supporting Information

The Supporting Information is available free of charge at https://pubs.acs.org/doi/10.1021/acsomega.1c04354.

Mass spectra obtained using a probe pulse with an intensity of 6.1×10^{13} W/cm^2 (PDF)

■ AUTHOR INFORMATION

Corresponding Authors

Akitaka Matsuda − *Department of Chemistry, Graduate School of Science, Nagoya University, Nagoya, Aichi 464-8602, Japan*; Email: amatsuda@chem.nagoya-u.ac.jp

Akiyoshi Hishikawa − *Department of Chemistry, Graduate School of Science, Nagoya University, Nagoya, Aichi 464-8602, Japan; Research Center for Materials Science, Nagoya University, Nagoya, Aichi 464-8602, Japan*; orcid.org/0000-0002-4147-294X; Email: hishi@chem.nagoya-u.ac.jp

Authors

Kentaro Tani − *Department of Chemistry, Graduate School of Science, Nagoya University, Nagoya, Aichi 464-8602, Japan*

Yukari Takeuchi − *Department of Chemistry, Graduate School of Science, Nagoya University, Nagoya, Aichi 464-8602, Japan*

Yui Hayakawa − *Department of Chemistry, Graduate School of Science, Nagoya University, Nagoya, Aichi 464-8602, Japan*

Complete contact information is available at: https://pubs.acs.org/10.1021/acsomega.1c04354

Notes

The authors declare no competing financial interest.

■ ACKNOWLEDGMENTS

The present study was supported by JSPS KAKENHI grant numbers JP26620004, JP17K05094, and JP21K03521.

■ REFERENCES

(1) Kling, M. F.; von den Hoff, P.; Znakovskaya, I.; de Vivie-Riedle, R. (Sub-)femtosecond control of molecular reactions via tailoring the electric field of light. *Phys. Chem. Chem. Phys.* **2013**, *15*, 9448−9467.

(2) Solá, I. R.; González-Vázquez, J.; de Nalda, R.; Bañares, L. Strong field laser control of photochemistry. *Phys. Chem. Chem. Phys.* **2015**, *17*, 13183−13200.

(3) Assion, A.; Baumert, T.; Bergt, M.; Brixner, T.; Kiefer, B.; Seyfried, V.; Strehle, M.; Gerber, G. Control of chemical reactions by feedback-optimized phase-shaped femtosecond laser pulses. *Science* **1998**, *282*, 919−922.

(4) Levis, R. J.; Menkir, G. M.; Rabitz, H. Selective bond dissociation and rearrangement with optimally tailored, strong-field laser pulses. *Science* **2001**, *292*, 709−713.

(5) Cardoza, D.; Baertschy, M.; Weinacht, T. Understanding learning control of molecular fragmentation. *Chem. Phys. Lett.* **2005**, *411*, 311−315.

(6) Lozovoy, V. V.; Zhu, X.; Gunaratne, T. C.; Harris, D. A.; Shane, J. C.; Dantus, M. Control of molecular fragmentation using shaped femtosecond pulses. *J. Phys. Chem. A* **2008**, *112*, 3789−3812.

(7) Endo, T.; Fujise, H.; Kawachi, Y.; Ishihara, A.; Matsuda, A.; Fushitani, M.; Kono, H.; Hishikawa, A. Selective bond breaking of CO_2 in phase-locked two-color intense laser fields: laser field intensity dependence. *Phys. Chem. Chem. Phys.* **2017**, *19*, 3550−3556.

(8) Hishikawa, A.; Matsuda, A.; Fushitani, M. Ultrafast reaction imaging and control by ultrashort intense laser pulses. *Bull. Chem. Soc. Jpn.* **2020**, *93*, 1293−1304.

(9) Chin, S. L.; Hosseini, S. A.; Liu, W.; Luo, Q.; Théberge, F.; Aközbek, N.; Becker, A.; Kandidov, V. P.; Kosareva, O. G.; Schroeder, H. The propagation of powerful femtosecond laser pulses in optical media: physics, applications, and new challenges. *Can. J. Phys.* **2005**, *83*, 863−905.

(10) Couairon, A.; Mysyrowicz, A. Femtosecond filamentation in transparent media. *Phys. Rep.* **2007**, *441*, 47−189.

(11) Bergé, L.; Skupin, S.; Nuter, R.; Kasparian, J.; Wolf, J.-P. Ultrashort filaments of light in weakly ionized, optically transparent media. *Rep. Prog. Phys.* **2007**, *70*, 1633−1713.

(12) Rohwetter, P.; Kasparian, J.; Stelmaszczyk, K.; Hao, Z.; Henin, S.; Lascoux, N.; Nakaema, W. M.; Petit, Y.; Queißer, M.; Salamé, R.; Salmon, E.; Wöste, L.; Wolf, J.-P. Laser-induced water condensation in air. *Nat. Photonics* **2010**, *4*, 451−456.

(13) du Plessis, A.; Strydom, C. A.; Uys, H.; Botha, L. R. Laser induced and controlled chemical reaction of carbon monoxide and hydrogen. *J. Chem. Phys.* **2011**, *135*, 204303.

(14) Ju, J.; Liu, J.; Wang, C.; Sun, H.; Wang, W.; Ge, X.; Li, C.; Chin, S. L.; Li, R.; Xu, Z. Laser-filamentation-induced condensation and snow formation in a cloud chamber. *Opt. Lett.* **2012**, *37*, 1214−1216.

(15) Shumlas, S. L.; Moore Tibbetts, K.; Odhner, J. H.; Romanov, D. A.; Levis, R. J.; Strongin, D. R. Formation of carbon nanospheres via ultrashort pulse laser irradiation of methane. *Mater. Chem. Phys.* **2015**, *156*, 47−53.

(16) Tibbetts, K. M.; Odhner, J.; Vaddypally, S.; Tangeysh, B.; Cerkez, E. B.; Strongin, D. R.; Zdilla, M. J.; Levis, R. J. Amorphous aluminum-carbide and aluminum-magnesium-carbide nanoparticles from gas phase activation of trimethylaluminum and octamethyldialuminummagnesium using simultaneous spatially and temporally focused ultrashort laser pulses. *Nano-Struct. Nano-Objects* **2016**, *6*, 1−4.

(17) Taguchi, Y.; Endo, H.; Kodama, T.; Achiba, Y.; Shiromaru, H.; Wakabayashi, T.; Wales, B.; Sanderson, J. H. Polyyne formation by ns and fs laser induced breakdown in hydrocarbon gas flow. *Carbon* **2017**, *115*, 169−174.

(18) Matsuda, A.; Hayashi, T.; Kitaura, R.; Hishikawa, A. Femtosecond laser filamentation in gaseous ethylene: formation of hydrogenated amorphous carbon. *Chem. Lett.* **2017**, *46*, 1426−1429.

(19) Takizawa, N.; Kodama, T.; Shiromaru, H.; Wakabayashi, T.; Al-Tuairqi, S.; Wang, Q.; Zhang, H.; Sanderson, J. H. Efficient polyyne formation by ns and fs laser-induced breakdown in ethylene and acetylene gas flow. *Carbon* **2019**, *152*, 372−375.

(20) Nakamura, T.; Mochidzuki, Y.; Sato, S. Fabrication of Gold Nanoparticles in Intense Optical Field by Femtosecond Laser Irradiation of Aqueous Solution. *J. Mater. Res.* **2008**, *23*, 968−974.

(21) Sato, Y.; Kodama, T.; Shiromaru, H.; Sanderson, J. H.; Fujino, T.; Wada, Y.; Wakabayashi, T.; Achiba, Y. Synthesis of polyyne molecules from hexane by irradiation of intense femtosecond laser pulses. *Carbon* **2010**, *48*, 1673−1676.

(22) Wesolowski, M. J.; Kuzmin, S.; Moores, B.; Wales, B.; Karimi, R.; Zaidi, A. A.; Leonenko, Z.; Sanderson, J. H.; Duley, W. W. Polyyne synthesis and amorphous carbon nano-particle formation by femtosecond irradiation of benzene. *Carbon* **2011**, *49*, 625−630.

(23) Yatsuhashi, T.; Uchida, N.; Nishikawa, K. Novel method of producing carbon nanoparticles on benzene/water interface with femtosecond laser plasma filament. *Chem. Lett.* **2012**, *41*, 722−724.

(24) Odhner, J. H.; Moore Tibbetts, K.; Tangeysh, B.; Wayland, B. B.; Levis, R. J. Mechanism of improved Au nanoparticle size distributions using simultaneous spatial and temporal focusing for femtosecond laser irradiation of aquaous $KAuCl_4$. *J. Phys. Chem. C* **2014**, *118*, 23986−23995.

(25) Zang, H.; Li, H.; Zhang, W.; Fu, Y.; Chen, S.; Xu, H.; Li, R. Robust and ultralow-energy-threshold ignition of a lean mixture by an ultrashort-pulsed laser in the filamentation regime. *Light: Sci. Appl.* **2021**, *10*, 49.

(26) Petit, Y.; Henin, S.; Kasparian, J.; Wolf, J.-P. Production of ozone and nitrogen oxides by laser filamentation. *Appl. Phys. Lett.* **2010**, *97*, 021108.

(27) Camino, A.; Li, S.; Hao, Z.; Lin, J. Spectroscopic determination of NO_2, NO_3 and O_3 temporal evolution induced by femtosecond filamentation in air. *Appl. Phys. Lett.* **2015**, *106*, 021105.
(28) Levin, L.; Skomorowski, W.; Rybak, L.; Kosloff, R.; Koch, C. P.; Amitay, Z. Coherent control of bond making. *Phys. Rev. Lett.* **2015**, *114*, 233003.
(29) Valle Brozas, F.; Salgado, C.; Apiñaniz, J. I.; Carpentier, A. V.; Sánchez Albaneda, M.; Roso, L.; Raposo, C.; Padilla, C.; Peralta Conde, A. Determination of the species generated in atmospheric-pressure laser-induced plasmas by mass spectrometry techniques. *Laser Phys.* **2016**, *26*, 055602.
(30) Casari, C. S.; Tommasini, M.; Tykwinski, R. R.; Milani, A. Carbon-atom wires: 1-D systems with tunable properties. *Nanoscale* **2016**, *8*, 4414−4435.
(31) Van Orden, A.; Saykally, R. J. Small Carbon Clusters: Spectroscopy, Structure, and Energetics. *Chem. Rev.* **1998**, *98*, 2313−2358.
(32) Kaiser, R. I. Experimental investigation on the formation of carbon-bearing molecules in the interstellar medium via neutral-neutral reactions. *Chem. Rev.* **2002**, *102*, 1309−1358.
(33) Bieri, G.; Burger, F.; Heilbronner, E.; Maier, J. P. Valence ionization enrgies of hydrocarbons. *Helv. Chim. Acta* **1977**, *60*, 2213−2233.
(34) Zhang, X.; Chen, P. Photoelectron spectrum of o-benzyne. Ionization potentials as a measure of singlet-triplet gaps. *J. Am. Chem. Soc.* **1992**, *114*, 3147−3148.
(35) Rosenstock, H. M.; Dannacher, J.; Liebman, J. F. The role of excited electronic states in ion fragmentation: $C_6H_6^+$. *Radiat. Phys. Chem.* **1982**, *20*, 7−28.
(36) Cradock, S.; Ebsworth, E. A. V.; Moretto, H.; Rankin, D. W. H. Photoelectron spectra and fluxional behaviour in some σ-cyclopentadienes. *J. Chem. Soc., Dalton Trans.* **1975**, 390−392.
(37) Carlier, P.; Mouvier, G.; Mesnard, D.; Miginiac, L. Etude par spectrometrie de photoelectrons de la structure electronique des enynes conjugues. *J. Electron Spectrosc. Relat. Phenom.* **1979**, *16*, 147−167.
(38) Ammosov, M. V.; Delone, N. B.; Kraĭnov, V. P. Tunnel ionization of complex atoms and of atomic ions in an alternating electromagnetic field. *Sov. Phys. JETP* **1986**, *64*, 1191−1194.
(39) Tong, X. M.; Zhao, Z. X.; Lin, C. D. Theory of molecular tunneling ionization. *Phys. Rev. A* **2002**, *66*, 033402.
(40) Endo, T.; Fujise, H.; Hasegawa, H.; Matsuda, A.; Fushitani, M.; Tolstikhin, O. I.; Morishita, T.; Hishikawa, A. Angle dependence of dissociative tunneling ionization of NO in asymmetric two-color intense laser fields. *Phys. Rev. A: At., Mol., Opt. Phys.* **2019**, *100*, 053422.
(41) Morishita, T.; Chen, Z.; Watanabe, S.; Lin, C. D. Two-dimensional electron momentum spectra of argon ionized by short intense lasers: Comparison of theory with experiment. *Phys. Rev. A* **2007**, *75*, 023407.
(42) Peng, J.; Puskas, N.; Corkum, P. B.; Rayner, D. M.; Loboda, A. V. High-pressure gas phase femtosecond laser ionization mass spectrometry. *Anal. Chem.* **2012**, *84*, 5633−5640.
(43) Casari, C. S.; Giannuzzi, C. S.; Russo, V. Carbon-atom wires produced by nanosecond pulsed laser deposition in a background gas. *Carbon* **2016**, *104*, 190−195.
(44) Talebpour, A.; Bandrauk, A. D.; Yang, J.; Chin, S. L. Multiphoton ionization of inner-valence electrons and fragmentation of ethylene in an intense Ti:sapphire laser pulse. *Chem. Phys. Lett.* **1999**, *313*, 789−794.
(45) Kong, F.; Luo, Q.; Xu, H.; Sharifi, M.; Song, D.; Chin, S. L. Explosive photodissociation of methane induced by ultrafast intense laser. *J. Chem. Phys.* **2006**, *125*, 133320.
(46) Bulgakov, A. V.; Mirza, I.; Bulgakova, N. M.; Zhukov, V. P.; Machulka, R.; Haderka, O.; Campbell, E. E. B.; Mocek, T. Initiation of air ionization by ultrashort laser pulses: evidence for a role of metastable-state air molecules. *J. Phys. D: Appl. Phys.* **2018**, *51*, 25LT02.
(47) Giroux, L.; Back, M. H.; Back, R. A. Photolysis of ethylene at 193 nm. *Can. J. Chem.* **1989**, *67*, 1166−1173.
(48) Xu, S.; Sun, X.; Zeng, B.; Chu, W.; Zhao, J.; Liu, W.; Cheng, Y.; Xu, Z.; Chin, S. L. Simple method of measuring laser peak intensity inside femtosecond laser filament in air. *Opt. Express* **2012**, *20*, 299−307.

https://doi.org/10.1021/acsomega.1c04354
ACS Omega 2021, 6, 29862−29868